

研究论文

帘线/橡胶复合材料各向异性黏-超弹性本构模型¹⁾黄小双 彭雄奇²⁾ 张必超

(上海交通大学材料科学与工程学院, 上海 200030)

摘要 帘线/橡胶复合材料广泛应用于轮胎等重要工程领域, 为了描述其在服役条件下的大变形、非线性、各向异性和高应变率等材料力学行为, 基于纤维增强复合材料连续介质力学理论, 提出了一种考虑应变率效应的帘线/橡胶复合材料各向异性黏-超弹性本构模型. 该模型中单位体积的应变能被解耦为便于参数识别的基体等容变形能、帘线拉伸变形能、剪切应变能和黏性应变能四部分. 给出了模型参数的确定方法, 并通过拟合文献中单轴拉伸、偏轴拉伸实验数据, 得到了模型参数. 利用该模型预测了不同加载和变形条件下的力学行为, 并将预测结果与实验结果对比分析. 结果表明, 考虑黏性模型和不考虑黏性模型对不同应变率变形条件下的预测结果相差很大, 且考虑黏性模型的预测结果与实验结果吻合很好. 因此, 与不考虑黏性模型相比, 所提出的各向异性黏-超弹性本构模型能更好地表征帘线/橡胶复合材料在大变形、高应变率条件下的力学特性.

关键词 帘线/橡胶复合材料, 各向异性, 黏-超弹性, 本构模型, 模型参数拟合

中图分类号: TB121, TB332 文献标识码: A doi: 10.6052/0459-1879-15-189

AN ANISOTROPIC VISCO-HYPERELASTIC CONSTITUTIVE MODEL FOR CORD-RUBBER COMPOSITES¹⁾Huang Xiaoshuang Peng Xiongqi²⁾ Zhang Bichao

(School of Materials Science and Engineering, Shanghai JiaoTong University, Shanghai 200030, China)

Abstract Based on fiber reinforced continuum mechanics theory, an anisotropic visco-hyperelastic constitutive model for cord-rubber composites was developed to characterize their highly non-linear, strongly anisotropic and strain rate dependent mechanical behaviors under high speed impact or large deformation condition. The unit-volume strain energy function for the visco-hyperelastic model was decomposed into four parts, representing the strain energy from isochoric rubber, the tensile energy from cord elongation, shearing energy from interaction between cord and rubber and viscous potential energy due to viscous characteristics, respectively, which greatly facilitated and simplified the identification of material parameters. By introducing the so called viscous potential energy that could not be neglected under particular loading conditions, the computation accuracy of the model was significantly improved. A simple approach for fitting the parameters was given. Experimental data from literature was used to identify material parameters in the constitutive for a specific cord-rubber composite. The developed model was validated by comparing numerical results with experimental uniaxial tension and bias-tension data under different strain rates, demonstrating that the developed constitutive model is highly suitable for characterizing the anisotropic and viscous material behaviors of cord-rubber composites under large deformation. The proposed model is simple, useful and easy for material parameter determination. It provides a theoretical

2015-05-27 收稿, 2015-09-16 录用, 2015-09-28 网络版发表.

1) 国家自然科学基金资助项目 (11172171).

2) 彭雄奇, 教授, 主要研究方向: 力学本构、复合材料结构设计、复合材料成型. E-mail: xqpeng@sjtu.edu.cn

引用格式: 黄小双, 彭雄奇, 张必超. 帘线/橡胶复合材料各向异性黏-超弹性本构模型. 力学学报, 2016, 48(1): 140-145

Huang Xiaoshuang, Peng Xiongqi, Zhang Bichao. An anisotropic visco-hyperelastic constitutive model for cord-rubber composites. *Chinese Journal of Theoretical and Applied Mechanics*, 2016, 48(1): 140-145

foundation for dynamic finite element analysis of tire in the future.

Key words cord-rubber composites, anisotropic, visco-hyperelastic, constitutive model, parameter determination

引言

帘线增强橡胶基复合材料是由帘线增强相和橡胶基体经过有效复合而形成的一种柔性复合材料, 广泛应用于轮胎、充气弹簧和传动带. 典型的子午线轮胎结构如图 1 所示, 胎体层主要由橡胶基体和钢丝帘线组成. 其基体是超弹性, 可以大变形; 帘线方向的拉伸模量远大于其他方向的拉伸模量而呈各向异性^[1]. 发展一种合适的本构模型来准确表征轮胎在服役条件下的大变形、非线性、各向异性和高应变率等力学特性具有重要的理论意义和工程应用价值.

尽管在这一领域已经有很多研究成果, 但都具有各自的局限性. 传统的线弹性理论不适用于大变形情况, 无法解决材料非线性、几何非线性和边界非线性等多重耦合问题^[1-3]. 基于微观力学理论的哈尔平-蔡 (Halpin-Tsai) 方程虽然可以预测沿帘线方向的力学性能, 但不能有效预测垂直帘线方向的力学性能和面内剪切性能^[4-6]. 加强筋模型^[7-9]和横观各向同性超弹性模型^[10-13]忽略了帘线和橡胶基体间的相互作用, 无法追踪帘线角度变化下的力学行为. 考虑帘线和橡胶基体间相互作用的各向异性超弹性模型不能描述轮胎在服役工况下的冲击和高应变率效应^[14-17]. 近年来, 一些学者分别针对帘线、橡胶及其复合材料进行了大量的实验研究, 有利于理解其在大变形和高速冲击下的力学行为, 但没有进一步对其进行本构化建模^[18-20]. 目前存在的黏-超弹性模型^[21-23]在每一组应变率条件下都需要测定相应的黏性系数, 模型复杂导致参数确定困难, 不具有普适性.

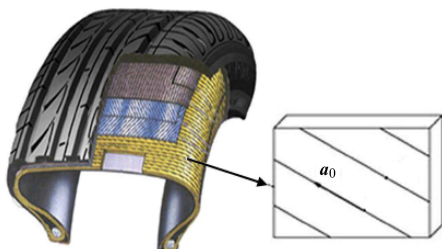


图 1 典型的子午线轮胎结构^[1]: 单层带束层帘线方向为 a_0

Fig. 1 Typical radial tire construction^[1]: a_0 represents the direction of a single belt cord

本文在作者前期提出的帘线/橡胶复合材料各向异性超弹性本构模型^[1]的基础上, 考虑轮胎在服役条件下的大变形、非线性和高应变率等工况特点, 建立一种能表征应变率效应的帘线/橡胶复合材料各向异性黏-超弹性本构模型.

1 各向异性黏-超弹性本构模型

1.1 本构模型的一般形式

基于连续介质力学理论, 对于黏性基体的纤维增强复合材料, 应变能函数可以分解为超弹性应变能和黏性应变能两部分^[24-26]

$$W(\mathbf{C}, \dot{\mathbf{C}}, \mathbf{a}_0) = W^e(\mathbf{C}, \mathbf{a}_0) + \psi^v(\mathbf{C}, \dot{\mathbf{C}}, \mathbf{a}_0) \quad (1)$$

式中, \mathbf{C} 为右柯西-格林 (Cauchy-Green) 应变张量, $\dot{\mathbf{C}}$ 为右柯西-格林应变率张量, \mathbf{a}_0 为纤维的初始单位方向向量.

超弹性应变能 W^e 可以表示为应变张量不变量 I_i ($i = 1, 2, 3, 4, 5$) 的标量函数, 即

$$W^e(\mathbf{C}, \mathbf{a}_0) = W^e(I_1, I_2, I_3, I_4, I_5) \quad (2)$$

右柯西-格林应变张量不变量分别为

$$\left. \begin{aligned} I_1 &= \mathbf{I} : \mathbf{C} = \text{tr}(\mathbf{C}) \\ I_2 &= \frac{1}{2} [(\text{tr}\mathbf{C})^2 - \text{tr}(\mathbf{C}^2)] \\ I_3 &= \det(\mathbf{C}) \\ I_4 &= \mathbf{A}_0 : \mathbf{C} = \mathbf{a}_0 \cdot \mathbf{C} \cdot \mathbf{a}_0 = \lambda_a^2 \\ I_5 &= \mathbf{A}_0 : \mathbf{C}^2 = \mathbf{a}_0 \cdot \mathbf{C}^2 \cdot \mathbf{a}_0 \end{aligned} \right\} \quad (3)$$

式中, \mathbf{I} 为二阶单位张量, 结构张量 $\mathbf{A}_0 = \mathbf{a}_0 \otimes \mathbf{a}_0$.

黏性应变能 ψ^v 也可以表示为应变率张量不变量 J_i ($i = 1, 2, 3, 4, 5$) 的标量函数, 即

$$W(\mathbf{C}, \dot{\mathbf{C}}, \mathbf{a}_0) = \psi^v(J_1, J_2, J_3, J_4, J_5) \quad (4)$$

右柯西-格林应变率张量不变量分别为

$$\left. \begin{aligned} J_1 &= \mathbf{I} : \dot{\mathbf{C}} = \text{tr}(\dot{\mathbf{C}}) \\ J_2 &= \frac{1}{2} (\mathbf{I} : \dot{\mathbf{C}}^2) = \frac{1}{2} \text{tr}(\dot{\mathbf{C}}^2) \\ J_3 &= \det(\dot{\mathbf{C}}) \\ J_4 &= \mathbf{A}_0 : \dot{\mathbf{C}} = \mathbf{a}_0 \cdot \dot{\mathbf{C}} \cdot \mathbf{a}_0 \\ J_5 &= \mathbf{A}_0 : \dot{\mathbf{C}}^2 = \mathbf{a}_0 \cdot \dot{\mathbf{C}}^2 \cdot \mathbf{a}_0 \end{aligned} \right\} \quad (5)$$

式中, λ_a 代表纤维(帘线)的拉伸比.

第二皮奥拉-基尔霍夫(Piola-Kirchhoff)应力张量 \mathbf{S} 由超弹性应力张量 \mathbf{S}^e 和黏性应力张量 \mathbf{S}^v 两部分组成

$$\mathbf{S} = \mathbf{S}^e + \mathbf{S}^v = 2 \left[\frac{\partial W^e}{\partial \mathbf{C}} + \frac{\partial \psi^v}{\partial \dot{\mathbf{C}}} \right] = 2 \left[\sum_{i=1}^5 \left(\frac{\partial W^e}{\partial I_i} \frac{\partial I_i}{\partial \mathbf{C}} \right) + \sum_{j=1}^5 \left(\frac{\partial \psi^v}{\partial J_j} \frac{\partial J_j}{\partial \dot{\mathbf{C}}} \right) \right] \quad (6)$$

1.2 超弹性应变能的解耦

超弹性应变能 W^e 可以解耦为便于参数识别的基体等容变形能 W_m^e 、帘线拉伸应变能 W_f^e 和剪切应变能 W_{shear} 三部分^[14,27]

$$W^e = W_m^e + W_f^e + W_{\text{shear}} = V_m W_m + V_f W_f + W_{\text{shear}} \quad (7)$$

式中, V_m, V_f 分别为橡胶和帘线的体积百分比.

1.2.1 基体等容变形能函数

假设基体为不可压缩材料, 结合约(Yeoh)模型^[28]和穆尼-里夫林(Mooney-Rivlin)模型^[29], 在不可压缩的假设下, 纯橡胶基体等容变形能选用多项式函数

$$W_m = \sum_{i=1}^2 C_{i0} (I_1 - 3)^i + \sum_{j=1}^2 D_{j0} (I_2 - 3)^j \quad (8)$$

式中, 基体材料参数 C_{i0} 和 D_{j0} 的单位均为 MPa.

1.2.2 帘线拉伸应变能函数

帘线的应变能与其拉伸有关, 忽略其压缩应变能, 则帘线拉伸应变能选用多项式函数^[30]

$$W_f = \begin{cases} \sum_{i=2}^4 C_i (I_4 - 1)^i, & I_4 > 1 \\ 0, & I_4 \leq 1 \end{cases} \quad (9)$$

式中, 材料参数 C_i ($i = 2, 3, 4$) 的单位均为 MPa.

1.2.3 帘线-橡胶剪切应变能函数

忽略帘线和橡胶基体间的正剪切作用^[17], 角剪切应变能 W_{shear} 可以表示为帘线和基体夹角变化 φ 的大小有关的函数^[14], 即

$$W_{\text{shear}} = W_{\text{shear}}(I_4, \chi) = f(I_4)(a\chi^2 + b\chi) \quad (10)$$

式中, $\chi = \tan^2 \varphi = \frac{I_4}{I_3} (I_5 - I_1 I_4 + I_2) - 1$ ^[14]. 剪切性能参数 a 和 b 的单位均为 MPa. 基于实验数据, 剪切影响因子 $f(I_4)$ 可以表示为

$$f(I_4) = \exp[c_1 (I_4 - 1)] \quad (11)$$

式中, c_1 为无量纲参数.

1.3 黏性应变能函数的推导

由帘线在不同应变率下的单向拉伸实验数据可知^[18], 帘线的应变率效应不明显, 所以忽略其影响, 只考虑基体黏性, 则黏性应变能函数可表示为应变张量不变量和应变率张量不变量的函数, 即

$$\psi^v = \psi^v(I_1, J_1) = g(J_1) \sum_{i=0}^2 \eta_i (I_1 - 3)^i \quad (12)$$

式中, $\sum_{i=0}^2 \eta_i (I_1 - 3)^i$ 反映基体变形, 黏性系数 η_0, η_1 和 η_2 的单位均为 MPa. 黏性影响因子 $g(J_1)$ 表征与率相关, 为了满足准静态条件下 $J_1 = 0$ 时, $g(J_1) = 0$ 的边界条件, 构造了如下对数函数形式

$$g(J_1) = \ln(c_2 J_1 + 1) \quad (13)$$

式中, 材料参数 c_2 的单位为 s.

1.4 帘线/橡胶黏-超弹性本构模型

已经分别确定了基体等容变形能、帘线拉伸变形能、剪切应变能和黏性应变能的函数形式, 而且每一部分能量的物理意义都非常明确. 将式(7)~(13)代入式(6), 并令 $W_i^e = \frac{\partial W^e}{\partial I_i}$, 则得到超弹性应力张量 \mathbf{S}^e 和黏性应力张量 \mathbf{S}^v 分别为

$$\mathbf{S}^e = 2 \left[(W_1^e + I_1 W_2^e) \mathbf{I} - W_2^e \mathbf{C} + W_4^e \mathbf{a}_0 \otimes \mathbf{a}_0 + W_5^e (\mathbf{a}_0 \otimes \mathbf{C} \cdot \mathbf{a}_0 + \mathbf{a}_0 \cdot \mathbf{C} \otimes \mathbf{a}_0) \right] \quad (14)$$

$$\mathbf{S}^v = 2c_2 \ln(c_2 J_1 + 1) \left(\sum_{i=0}^2 \eta_i (I_1 - 1)^i \right) \mathbf{I} \quad (15)$$

通过最小二乘法拟合单轴拉伸和偏轴拉伸实验数据, 可以确定本构模型参数, 下面给出模型参数的确定方法:

(1) 拟合纯橡胶的准静态单轴拉伸实验数据得到橡胶的材料参数 C_{i0} 和 D_{i0} 。

(2) 拟合纯帘线的准静态单轴拉伸实验数据得到帘线的材料参数 C_i ($i = 2, 3, 4$)。

(3) 由 (1) 和 (2) 两步得到 C_i , C_{i0} 和 D_{i0} 后, 拟合准静态偏轴拉伸实验数据得到角剪切应变能密度函数 W_{shear} 的参数 a, b 和 c_1 。

(4) 根据前面 3 步得到的材料参数, 拟合高应变率拉伸条件下的实验数据得到与率相关的黏性系数 η_0, η_1 和 η_2 和材料参数 c_2 。

2 本构模型的参数确定

2.1 模型应用于单轴拉伸

对于不同帘线角度的单轴拉伸, 如图 2 所示, 假设变形前帘线的单位方向向量为

$$\mathbf{a}_0 = [\cos \alpha \quad \sin \alpha \quad 0] \quad (16)$$

变形梯度张量 \mathbf{F} 、格林应变张量 \mathbf{C} 和应变率张量 $\dot{\mathbf{C}}$ 分别为

$$\left. \begin{aligned} \mathbf{F} &= \text{dig} [\lambda_1 \quad \lambda_2 \quad \lambda_3] \\ \mathbf{C} &= \mathbf{F}^T \cdot \mathbf{F} = \text{dig} [\lambda_1^2 \quad \lambda_2^2 \quad \lambda_3^2] \\ \dot{\mathbf{C}} &= \dot{\mathbf{F}}^T \cdot \mathbf{F} + \mathbf{F}^T \cdot \dot{\mathbf{F}} = \text{dig} [2\lambda_1\dot{\lambda}_1 \quad 2\lambda_2\dot{\lambda}_2 \quad 2\lambda_3\dot{\lambda}_3] \end{aligned} \right\} \quad (17)$$

式中, λ_i 表示第 i 个主方向的拉伸比; 不变量 I_1, I_2, I_3, I_4, I_5 和 J_1 的表达式为

$$\left. \begin{aligned} I_1 &= \lambda_1^2 + \lambda_2^2 + \lambda_3^2 \\ I_2 &= \lambda_1^2\lambda_2^2 + \lambda_2^2\lambda_3^2 + \lambda_1^2\lambda_3^2 \\ I_3 &= \lambda_1^2\lambda_2^2\lambda_3^2 \\ I_4 &= \lambda_1^2 \cos^2 \alpha + \lambda_2^2 \sin^2 \alpha \\ I_5 &= \lambda_1^4 \cos^2 \alpha + \lambda_2^4 \sin^2 \alpha \\ J_1 &= 2(\lambda_1\lambda_1 + \lambda_2\lambda_2 + \lambda_3\lambda_3) \end{aligned} \right\} \quad (18)$$

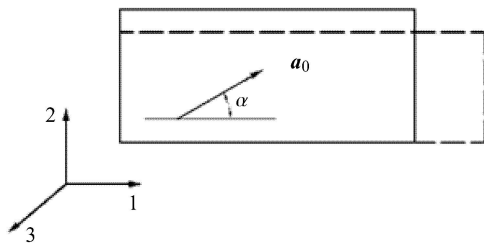


图 2 单层帘线/橡胶复合材料单轴拉伸变形
Fig. 2 Uniaxial tensile deformation of one family of cord reinforced composites

对于近似不可压缩材料的单轴拉伸变形, 可将 $I_5 - I_4^2$ 看作 χ 的主要部分^[14], 即 $\chi \approx I_5 - I_4^2$. 则沿拉伸方向的第二皮奥拉-基尔霍夫应力

$$\mathbf{S}_{11}^c = 2[W_1^c \mathbf{I} + W_2^c (I_1 - \lambda_1^2) + (W_4^c + 2W_5^c \lambda_1^2) \cos^2 \alpha] \quad (19)$$

$$\mathbf{S}_{11}^v = 2c_2 \ln(c_2 J_1 + 1) \sum_{i=0}^2 \eta_i (I_1 - 3)^i \quad (20)$$

将第二皮奥拉-基尔霍夫 (Piola-Kirchhoff) 应力 \mathbf{S} 转化为工程应力 \mathbf{P}

$$\mathbf{P} = \mathbf{S} \cdot \mathbf{F}^T \quad (21)$$

2.2 本构模型参数拟合

2.2.1 橡胶基体材料参数

由于缺少纯橡胶的单轴拉伸实验数据, 因此忽略帘线与基体正剪切作用^[14,17], 拟合与帘线方向垂直的准静态单轴拉伸实验数据^[18], 如图 3 所示, 可得到橡胶基体材料参数

$$\left. \begin{aligned} C_{10} &= 7.2449 \text{ MPa}, \quad C_{20} = 2.1952 \text{ MPa} \\ D_{10} &= -3.6129 \text{ MPa}, \quad D_{20} = -1.9871 \text{ MPa} \end{aligned} \right\} \quad (22)$$

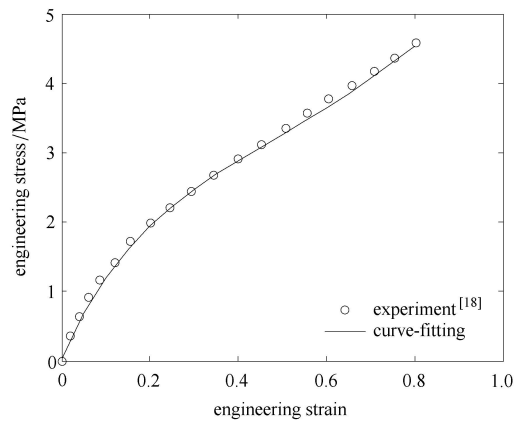


图 3 横向单轴拉伸应力-应变曲线

Fig. 3 Stress-strain curve of transverse tension

2.2.2 帘线拉伸材料参数

拟合纯帘线准静态单轴拉伸实验数据^[18], 如图 4 所示, 可得到帘线材料参数

$$C_2 = 12434 \text{ MPa}, \quad C_3 = 148 \text{ MPa}, \quad C_4 = 3 \text{ MPa} \quad (23)$$

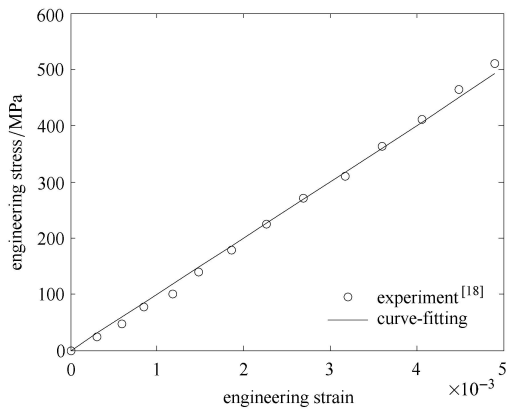


图 4 帘线单轴拉伸应力-应变曲线

Fig. 4 Uniaxial tensile stress-strain curve of pure cord

2.2.3 剪切应变能参数

得到基体材料参数 C_{i0} 和 D_{i0} , 帘线材料参数 C_i 以后, 在体积百分比 $V_m = 0.8$ 和 $V_f = 0.2$ 的条件下^[18], 将应变率为 0.0033 s^{-1} 假设为准静态拉伸, 拟合该应变率下与帘线成 45° 夹角的偏轴拉伸实验数据^[18], 如图 5 所示, 得到剪切性能参数

$$a = 0.2743\text{ MPa}, b = 0.3882\text{ MPa}, c_1 = -0.6601 \quad (24)$$

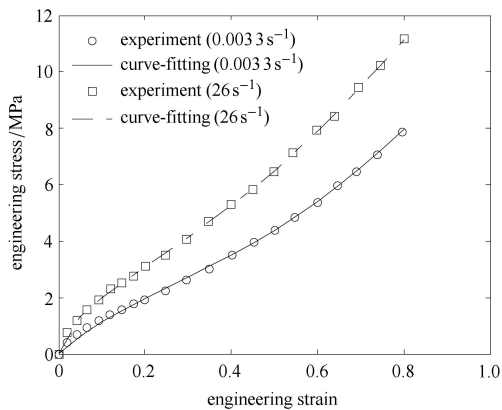


图 5 应变率为 0.0033 s^{-1} 和 26 s^{-1} 的偏轴拉伸应力-应变曲线

Fig. 5 Stress-strain curve of 45° off-axis tension under strain rate 0.0033 s^{-1} and 26 s^{-1}

2.2.4 黏性应变能参数

得到基体材料参数、帘线材料参数和剪切性能参数后, 拟合应变率为 26 s^{-1} 与帘线成 45° 夹角的偏轴拉伸实验数据^[18], 如图 5 所示, 得到与率相关的黏性应变能参数

$$\left. \begin{aligned} \eta_0 &= 0.0157\text{ MPa}, \eta_1 = 0.0138\text{ MPa} \\ \eta_2 &= -0.0038\text{ MPa}, c_2 = 5.2368\text{ s} \end{aligned} \right\} \quad (25)$$

3 本构模型验证及结果讨论

分别对应变率为 1.2 s^{-1} 和 131 s^{-1} 和 $g(J_1) = 0$ 条件下对帘线呈 45° 角的偏轴拉伸进行预测, 并将预测值与实验值^[18] 进行对比.

如图 6 所示, 应变率为 1.2 s^{-1} 和 131 s^{-1} 时, 考虑黏性和不考虑黏性预测结果相差很大, 且考虑黏性的预测结果与实验结果吻合度很好, 不考虑黏性的预测结果与准静态下实验数据一致, 因此证明了该帘线/橡胶复合材料各向异性黏-超弹性本构模型的准确性和有效性.

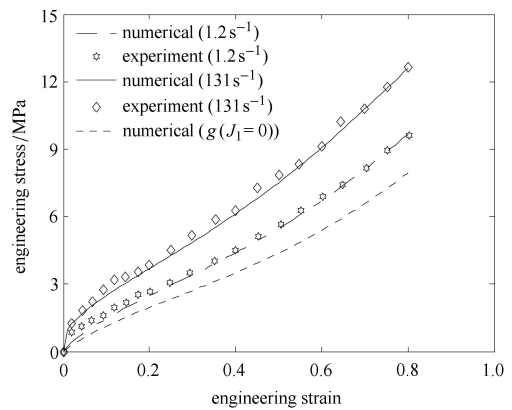


图 6 不同应变率下的偏轴拉伸应力-应变曲线

Fig. 6 Stress-strain curve of 45° off-axis tension under different strain rates

4 结 论

(1) 基于连续介质力学理论, 提出了一种帘线/橡胶复合材料各向异性黏-超弹性本构模型来描述轮胎胎体层在服役条件下的大变形、非线性和高应变率力学行为.

(2) 单位体积的应变能被解耦为便于参数识别的基体等容变形成能、帘线拉伸应变能、剪切应变能和黏性应变能四部分, 给出了模型参数的确定方法.

(3) 拟合出了本构模型参数, 并验证了模型的准确性和有效性. 这一本构模型具有简单实用、材料参数容易确定的优点, 为整体轮胎的动力学有限元分析奠定了基础.

参 考 文 献

1 郭国栋, 彭雄奇, 赵宁. 一种考虑剪切作用的各向异性超弹性本构模型. 力学学报, 2013, 45(3): 451-455 (Guo Guodong, Peng Xiongqi, Zhao Ning. An anisotropic hyperelastic constitutive model

- with shear interaction for cord-rubber tire composites. *Chinese Journal of Theoretical and Applied Mechanics*, 2013, 45(3): 451-455 (in Chinese))
- 2 Akasaka T, Kabe K, Sako K. Bending stiffness of a tire-belt structure with steel cords. *Composites Science and Technology*, 1985, 24(3): 215-230
 - 3 Clark SK. Theory of the elastic net applied to cord-rubber composites. *Rubber Chemistry and Technology*, 1983, 56(2): 372-389
 - 4 Affdl J, Kardos J. The Halpin-Tsai equations: A review. *Polymer Engineering & Science*, 1976, 16(5): 344-352
 - 5 Mansor M, Sapuan S, Zainudin E, et al. Rigidity analysis of kenaf thermoplastic composites using Halpin-Tsai equation. In: Proc. of Conference of in Applied Mechanics and Materials, 2014: 29-33
 - 6 Giner E, Vercher A, Marco M, et al. Estimation of the reinforcement factor ξ for calculating E2 with the Halpin-Tsai equations using the finite element method. *Composite Structures*, 2015, 124: 402-408
 - 7 Helnwein P, Liu CH, Meschke G, et al. A new 3-D finite element model for cord-reinforced rubber composites—application to analysis of automobile tires. *Finite Elements in Analysis and Design*, 1993, 14(1): 1-16
 - 8 Meschke G, Helnwein P. Large-strain 3D-analysis of fibre-reinforced composites using rebar elements: Hyperelastic formulations for cords. *Computational Mechanics*, 1994, 13(4): 241-254
 - 9 Yanjin G, Guoqun Z, Gang C. 3-dimensional non-linear FEM modeling and analysis of steady-rolling of radial tires. *Journal of Reinforced Plastics and Composites*, 2011, 30(3): 229-240
 - 10 Itskov M, Aksel N. A class of orthotropic and transversely isotropic hyperelastic constitutive models based on a polyconvex strain energy function. *International Journal of Solids and Structures*, 2004, 41(14): 3833-3848
 - 11 Brown LW, Smith LM. A simple transversely isotropic hyperelastic constitutive model suitable for finite element analysis of fiber reinforced elastomers. *Journal of Engineering Materials and Technology*, 2011, 133(2): 021021
 - 12 Ciarletta P, Izzo I, Micera S, et al. Stiffening by fiber reinforcement in soft materials: A hyperelastic theory at large strains and its application. *Journal of the Mechanical Behavior of Biomedical Materials*, 2011, 4(7): 1359-1368
 - 13 王友善, 王锋, 王浩. 超弹性本构模型在轮胎有限元分析中的应用. *轮胎工业*, 2009, 29(5): 277-282 (Wang Youshan, Wang Feng, Wang Hao. Application of hyperelastic constitutive models in finite element analysis on tires. *Tire Industry*, 2009, 29(5): 277-282 (in Chinese))
 - 14 Peng X, Guo Z, Moran B. An anisotropic hyperelastic constitutive model with fiber-matrix shear interaction for the human annulus fibrosus. *Journal of Applied Mechanics*, 2006, 73(5): 815-824
 - 15 Brieu M, Diani J, Bhatnagar N. A new biaxial tension test fixture for uniaxial testing machine-A validation for hyperelastic behavior of rubber-like materials. *Journal of Testing and Evaluation*, 2007, 35(4): 364
 - 16 Aboshio A, Green S, Ye J. New constitutive model for anisotropic hyperelastic biased woven fibre reinforced composite. *Plastics, Rubber and Composites*, 2014, 43(7): 225-234
 - 17 Guerin HL, Elliott DM. Quantifying the contributions of structure to annulus fibrosus mechanical function using a nonlinear, anisotropic, hyperelastic model. *Journal of Orthopaedic Research*, 2007, 25(4): 508-516
 - 18 Eiamnipon N, Nimdum P, Renard J, et al. Experimental investigation on high strain rate tensile behaviors of steel cord-rubber composite. *Composite Structures*, 2013, 99: 1-7
 - 19 Choi SS, Kim OB. Influence of specimen directions on recovery behaviors from circular deformation of polyester cord-inserted rubber composites. *Journal of Industrial and Engineering Chemistry*, 2014, 20(1): 202-207
 - 20 Rao S, Daniel IM, Gdoutos EE. Mechanical properties and failure behavior of cord/rubber composites. *Applied Composite Materials*, 2004, 11(6): 353-375
 - 21 Zhang F, Kuang Z, Wan Z, et al. Viscoelastic constitutive model of cord-rubber composite. *Journal of Reinforced Plastics and Composites*, 2005, 24(12): 1311-1320
 - 22 Shim V, Yang L, Lim C, et al. A visco-hyperelastic constitutive model to characterize both tensile and compressive behavior of rubber. *Journal of Applied Polymer Science*, 2004, 92(1): 523-531
 - 23 Anani Y, Alizadeh Y. Visco-hyperelastic constitutive law for modeling of foam's behavior. *Materials & Design*, 2011, 32(5): 2940-2948
 - 24 Zhurov AI, Evans SL, Holt CA, et al. A nonlinear compressible transversely-isotropic viscohyperelastic constitutive model of the periodontal ligament. In: Proc. of ASME 2008 International Mechanical Engineering Congress and Exposition, 2008: 707-719
 - 25 Spencer AJM. *Continuum Theory of the Mechanics of Fibre-reinforced Composites*. New York: Springer, 1984
 - 26 Jiang Y, Wang Y, Peng X. A visco-hyperelastic constitutive model for human spine ligaments. *Cell Biochemistry and Biophysics*, 2015, 71(2): 1147-1156
 - 27 彭雄奇, 王宇. 腰椎椎间植骨融合有限元分析. *力学学报*, 2011, 43(2): 381-389 (Peng Xiongqi, Wang Yu. Finite element analysis on lumbar interbody fusion. *Chinese Journal of Theoretical and Applied Mechanics*, 2013, 45(3): 451-455 (in Chinese))
 - 28 Yeoh O. Characterization of elastic properties of carbon-black-filled rubber vulcanizates. *Rubber Chemistry and Technology*, 1990, 63(5): 792-805
 - 29 Holzapfel GA, Gasser TC. A viscoelastic model for fiber-reinforced composites at finite strains: continuum basis, computational aspects and applications. *Computer Methods in Applied Mechanics and Engineering*, 2001, 190(34): 4379-4403
 - 30 Peng X, Guo Z, Du T, et al. A simple anisotropic hyperelastic constitutive model for textile fabrics with application to forming simulation. *Composites Part B: Engineering*, 2013, 52: 275-281

(责任编辑: 冯西桥)

(责任编辑: 刘希国)